USE OF THERMAL BANDS FOR LAND COVER ASSESSMENT:
CASE STUDY OF JHARIA COAL FIELD

Rashi Agarwal

Department of Information Technology
University Institute of Engineering and Technology
CSJM University, Kanpur, U.P, India

Abstract:

The growing pressure of population coupled with in-creasing variety of demands made on land resources, have brought extra pressure on the available land resources all over the country. Hence, in order to use land optimally, it is not only necessary to have the information on existing land use/land cover but also the capability to monitor the dynamics of land use resulting out of changing demands of increasing population. We have determined the land cover of Jharia region using clustering based on maximum likelihood algorithm for classification of an image of IRS (Indian Remote Sensing) –LISS III, 2010. A cost effective land cover classification (as NOAA AVHRR data is free of cost) has been performed using NOAA AVHRR data to assess the land cover, as well. 20 images of NOAA AVHRR spread over the year 2010 have been studied for land cover. 10 images are daytime images while the rest 10 are the corresponding night time images. We have then carried out regression analysis to determine the temperatures for assessment of the land cover on these 20 images. An accuracy of 70.1% is got for classification using just the thermal bands to determine the land cover.

1. Introduction

Conventional ground methods of land use mapping are labor intensive, time consuming and are done relatively infrequently. These maps soon become outdated with passage of time, particularly in a rapidly changing environment. In recent years, satellite remote sensing techniques have been developed, which have proved to be of immense value for preparing accurate land use/land cover maps and monitoring changes at regular intervals of time. In case of inaccessible region, this technique is perhaps the only method of obtaining the required data on a cost and time-effective basis.

The study of global change can be easily done by mapping, quantifying and monitoring changes in the physical characteristics of land cover (Henderson-Sellers and Pitman 1992). To carry out such studies space observations from satellite in visible (VIS), near-infrared (NIR) and thermal infrared (TIR) bands prove to be an attractive method. The initial works on land cover mapping (Tucker *et al.* 1985, Townshend *et al.* 1987, Loveland *et al.* 1991) and land cover change analysis (Nelson and Holben 1986, Tucker *et al.* 1991, Lambin and Strahler 1994) were based on the analysis of multi-temporal Normalized Difference Vegetation Index (NDVI) series produced by the National Oceanic and Atmospheric Administration (NOAA) from Advanced Very High Resolution Radiometer (AVHRR) images.The applications of mapping and monitoring land surfaces from satellite data combine information in the VIS/NIR bands in terms of NDVI and in the TIR bands (AVHRR Channels 4 and 5) in terms of the Land Surface Temperature (LST)(Lambin and Ehrlich,1995). A biophysical justification for the combination of LST and vegetation indices time series for land cover mapping and land cover change analysis was given in 1996 (Lambin and Ehrlich) . Using pixel-based based image analysis on Landsat Thematic Mapper(TM) data, Huang et al. (2002) compared thematic mapping accuracies produced using four different classification algorithms: support vector machines (SVMs), decision trees (DTs), a neural network classifier, and the maximum likelihood classifier (MLC). Their results suggested that the accuracy of SVM-based classifications generally outperformed the other three classification algorithms. Pal (2005) compared the accuracies of two supervised classification algorithms using Landsat Enhanced Thematic Mapper (ETM+) data: SVMs and Random Forests

(RFs) (Breiman, 2001), and found that they performed equally well. Gislason et al. (2006) compared a RF approach to a variety of decision tree-like algorithms using pixel-based image analysis of Landsat MSS data. In a recent study, Dingle Robertson and King (2011)compared pixel-based and object-based image analysis for classifying broad agricultural land cover types for two time periods (1995 and 2005) using Landsat-5 TM imagery. They compared land cover maps produced using MLC (pixel-based) and K-NN (object-based) algorithms and found that the difference in overall accuracy between these classification approaches was not statistically significant. Despite these findings, an intensive visual analysis of their post-classification analysis revealed that the object-based classification using K-NN depicted areas of change more accurately than the pixel-based classification using MLC.

A huge archive of images from the AVHRR are available for a 17-year period beginning in 1981, that can be used to produce global and regional maps of land use and land cover change. Hence, the objective of the present work is to examine the possibilities of using NOAA AVHRR multi-temporal imagery for mapping land cover.

2. Theory

2.1 Land Surface Temperature (LST): Remote Sensing in the Thermal Infrared part of the spectrum is concerned with radiation emitted by the Earth's surface and the atmosphere. The basic problem is the conversion of this radiance into temperature. The retrieval of surface temperatures from space has been studied since 1970s. Various methods have been proposed to correct the atmospheric contamination of the signal in thermal infrared. LST determinations from satellite data are mainly influenced by the atmosphere and surface emissivity; if both effects are not corrected for, the error in the LST may be very large (up to 12K).

The most popular method for estimation of LST is the split window method which is primarily use to analyse the NOAA AVHRR data. Sobrino *et al.* (1996) gave the following split window algorithm

$$\text{LST} = T_4 + A\ (T_4 - T_5) - B_0 + (1-\varepsilon)\ B_1 - \Delta\varepsilon\ B_2 \qquad\qquad (1)$$

where T_4 and T_5 are the brightness temperatures measured in AVHRR Channels 4 and 5 respectively, $\varepsilon = (\varepsilon_4 + \varepsilon_5)/2$ and $\Delta\varepsilon = \varepsilon_4 - \varepsilon_5$ are, respectively, the average effective emissivity in both channels and the spectral variation of emissivity. A, B_0, B_1 and B_2 are the split-window coefficients given by

$$A = (1 - \tau_4(\theta))/(\tau_4(\theta) - \tau_5(\theta)) \tag{2}$$

$$B_O = A[1 - \tau_4(\theta)](T_{a4} - T_{a5}) \tag{3}$$

$$B_1 = [1 - \tau_4(\theta)\tau_4(53)](T_4 - T_5)/(\tau_4(\theta) - \tau_5(\theta)) + \tau_4(53)T_4/4.667 \tag{4}$$

$$B_2 = \tau_5(\theta)AB_1 \tag{5}$$

T_{a4} and T_{a5} being the effective atmospheric temperatures in AVHRR Channels 4 and 5 respectively, and $\tau_4(\theta)$, $\tau_5(\theta)$ and $\tau_4(53)$ the total atmospheric path transmittances in Channels 4 and 5 respectively at zenith angle θ and in the 53° view direction.

We applied the operational split-window algorithm to approximate LST from NOAA AVHRR imagery given by Becker and Li (1990). This method takes advantage of the different absorption in two adjacent spectral windows, centered at 10.8 μm and 12 μm for the AVHRR instrument to correct the atmospheric effects. It describes the surface temperature in terms of simple linear combination of brightness temperatures measured in both the thermal channels. The brightness temperature incorporates the surface emissivity variation.

$$Ts = T4 + \delta w + \delta \varepsilon \tag{6}$$

Where δw and $\delta \varepsilon$ are water vapor and emissivity corrections respectively (Gutman, 1994)

$$\delta w = 2.63(T4 - T5) + 1.274 \tag{7}$$

$$\delta \varepsilon = [0.078(T4 + T5) + 1.69(T4 - T5)](1 - \varepsilon)/\varepsilon \tag{8}$$

2.2 Surface Emissivity: In order to apply eq. 1, the effective surface emissivity, ε, must be calculated. Here the following procedure was used for application to The Global Land 1-km AVHRR Project dataset.

Mixed pixels: For NDVI values between 0.2 and 0.5, a theoretical approach was used which models a given surface by considering it as being a mixture of bare soil and vegetation according to (Sobrino *et al.* 1990):

$$\varepsilon = (\varepsilon_4 + \varepsilon_5)/2 = 0.971 + .081 P_v \qquad (9)$$
$$\Delta\varepsilon = \varepsilon_4 - \varepsilon_5 = 0.006\,(1 - P_v)$$

where ε_4 and ε_5 are the emissivities of AVHRR channel 4 and channel 5 respectively, P_v is the proportion of vegetation given by

$$P_v = \frac{(NDVI - NDVI_{min})^2}{(NDVI_{max} - NDVI_{min})^2} \qquad (10)$$

Bare Soil pixels: For NDVI < 0.2
$$\varepsilon = 0.980 - 0.041\,\rho_1 \qquad (11)$$
$$\Delta\varepsilon = -0.003 - 0.029\,\rho_1$$
where ρ_1 is the AVHRR channel 1 reflectivity.

Fully Vegetated Pixels : For NDVI > 0.5
$$\varepsilon = \varepsilon_4 = \varepsilon_5 = 0.990 \qquad (12)$$

3. Area of Study and Satellite Data

3.1 JCF

The Jharia coal field, the largest coalfield in India, is located about 250 km NW of Calcutta and about 1150 km SE of Delhi (figure 1). This
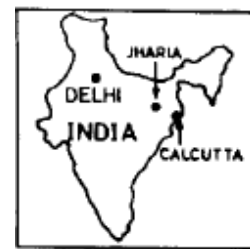

Fig.1: Location of JCF

coalfield lies between latitudes 23º 38' N and 23º 50' N, longitudes 86º 07'E and 86º 30'E covering an area of approximately 450 sq-km. The field is roughly sickle-shaped, with its longer axis running northwest-southeast.

3.2 Data Used

3.2.1 NOAA AVHRR

The AVHRR is a broad-band scanner that consists of four to five bands depending on the models of the sensor on board NOAA Satellites. AVHRR data are archived in three formats: HRPT (1.1 km spatial resolution at satellite nadir), LAC (1.1 km spatial resolution at satellite nadir), and GAC (4 km spatial resolution) formats. The AVHRR sensor provides global, pole to pole, data from all spectral channels. The swath width is 2399 km with 2048 pixels per scan line. The entire Earth can be covered in just 14.5 days. The advantage of the NOAA AVHRR LAC data are: synoptic coverage and hence low data volume (swath width 2700 km), high radiometric resolution (10 bit), relatively low cost (Free!, only handling cost), twice daily coverage and hence high possibilities of having cloud free data. The major disadvantages are: coarse spatial resolution (1.1 km at the nadir), preprocessing is time consuming, the methodology is not well developed, and LAC data has limited capability to record on-board. Designated originally for meteorological studies, AVHRR data can be used for various land applications, such as land cover assessment and monitoring. Due to the coarse spatial resolution (1 km), the pixel might represent different land cover types on the ground, but the spectral characteristic will be representation of the predominant cover type within that pixel. The minimum mapping unit for the NOAA AVHRR data is one square kilometer.

3.2.2   Indian Remote Sensing (IRS) Systems

The Indian Space Research Organisation (ISRO) has launched several IRS satellites: IRS-1A on March 17,1988, IRS-1B on August 29, 1991, IRS-1C in 1995 and IRS-1D in September 1997.

The sensors onboard the satellite utilize linear array sensor technology. The IRS data are marketed through Space Imaging Inc., in the United States.

The IRS-IC and ID satellites carry three sensors namely: the LISS – III multi-spectral sensor, a panchromatic sensor, and a Wide Field Sensor (WiFs). The LISS-III has four bands with the green, red, and near-infrared bands at 23x23 m spatial resolution and the short-wavelength infrared (SWIR) band at 70x70 m spatial resolution. The swath width is 142 km for bands 2,3 and 4 and 148 km for band 5. Repeat coverage is every 24 days at the equator.

4. Methodology

The study area was covered by six Survey of India topographical maps on 1:25,000 scale, numbered 73I/1SE, 73I/2NE, 73I/5SW, 73I/6NW, 73I/5SE and 73I/6NE. These maps were scanned, digitised and registered for further use.

Ten sets of the NOAA AVHRR data covering JCF were downloaded from Satellite Archive (SAA) of NOAA for processing. The digtial data of NOAA AVHRR in LAC formats were used in the present study. Preprocessing was carried out for all the datasets. The NOAA AVHRR data pre-processing comprises of data extraction and noise removal, radiometric calibration, geometric correction and cloud masking procedures. Indian Remote Sensing (IRS) Linear Imaging Self Scanning Sensors (LISS-III) imagery was used as the base image owing to its high spatial resolution. The data set are resampled to one square kilometer spatial resolution after geometric correction. Spectral characteristics of the individual bands, NDVI, and color composites were studied for land cover mapping.

4.1 Processing of images

4.1.1 IRS Image

The IRS image was calibrated and geo-referenced for further use. Spectral characteristics of the individual bands, NDVI and color composites were studied for land cover mapping. Unsupervised digital land cover classification was performed using spectral signature definition

by iterative clustering technique and maximum likelihood classification method. Interactive labeling of this signature information into major land cover categories was done.

Table 1. IRS spectral ranges, their combinations and applications

Channel Number/ Channel combination	Wave Length (μm)	Spectrum	Applications
2	0.52 - 0.59	Visible(green)	Discriminating clouds, Daytime cloud and surface features mapping.
3	0.62 – 0.68	Visible (Red)	Mapping land / water discrimination (water has lesser reflectance than other land uses), discriminating daytime cloud.
4	0.77-0.86	Near Infra Red	Determining temperature of radiating surface, night cloud mapping
5	1.55 -1.70	Short Wave Infra red	Determining sea surface temperature, day/night cloud mapping
NDVI = ((4-3)/(4+3))	NDVI Normalized Difference Vegetation Index	Vegetation Index is ratio or difference of reflectance value in the visible (Red) and Near Infra Red region of the spectrum	
FCC = R2:G1:B1	FCC False Color Composite	Generated by compositing three multi-band images with the use of three primary colours: by assigning blue to Reflected Visible band, green to Reflected Visible, and red to Visible/Near-Infrared band.	Green vegetations appears in different tones of red color. Snow & ice appears in white.

FCC = R1:G2:B1	FCC False Color Composite	Generated by compositing three multi-band images with the use of three primary colours: by assigning blue to Reflected Visible band, green to Visible/Near-Infrared band., and red to Reflected Visible.	Green vegetations appears in different tones of green color.

1.1.2   NOAA AVHRR Images

Day and night time NOAA AVHRR thermal band data (band 3, 4, 5 received in December 2010 covering JCF area are used to evaluate land surface temperature. Each pixel size of AVHRR is around 1.1 km x 1.1 km. Land use map of JCF including eight categories (Settlement, Agriculture land, Degraded vegetation, Forest, Fallow land, Barren land, Stream/River, Active mining area (Quarries + Over barren dumps)) is also used to assess surface temperature dependency on land cover   types.

4.2 Registration

Geometrical rectification of night time NOAA AVHRR thermal band data and land-use JCF was made by polynomial transformation, using more than five ground points on the river basin of Damodar, using day time NOAA AVHRR thermal band data which was rectified using UTM map projections. Since the pixel size of these data are different, the pixel size of land-use data is resampled to that of the NOAA AVHRR data (1.1 km x 1.1 km) using majority data as the value for   the   pixel   after   transformation.

4.3 Calculation of surface temperature

Using eq. 1 Land surface Temperature was calculated for the day and night images of NOAA AVHRR. The difference in temperature between day and night is calculated using the thermal band data as follows;

$$\Delta T_i = T_{di} - T_{ni} \qquad (4.1)$$

ΔTi: the difference of temperature between day and night for each pixel of band i

Tdi = day time LST temperature for each pixel of band i

Tni : night time LST temperature for each pixel of band i.

For each category of land use, distribution and average of ΔTi is calculated for band 4 in NOAA AVHRR.

5. Results and Discussions

The various images (Figure 2 – Figure 9) have been studied. Unsupervised clustering was performed on all the 20 images to obtain 9 different classes namely Settlement, Agricultural Land, Sparse vegetation, Degraded vegetation, Barren land, Tanks/Ponds, Stream/River ans Active mining area (Quarries+OB dumps). Each pixel was classified according to the Maximum Likelihood principal.

Maximum likelihood classification assumes that the statistics for each class in each band are normally distributed and calculates the probability that a given pixel belongs to a specific class. Unless you select a probability threshold, all pixels are classified. Each pixel is assigned to the class that has the highest probability (that is, the maximum likelihood). If the highest probability is smaller than a threshold you specify, the pixel remains unclassified.

ENVI implements maximum likelihood classification by calculating the following discriminant functions for each pixel in the image (Richards, 1999):

$$g,(x) = \ln p(\omega_i) - 1/2\ln|\Sigma_i| - 1/2(x - m_i)^T \sum_i^{-1}(x - m_i)$$

Where:

i = class

x = n-dimensional data (where n is the number of bands)

$p(\omega_i)$ = probability that class ω_i occurs in the image and is assumed the same for all classes

$|\Sigma i|$ = determinant of the covariance matrix of the data in class ω_i

$\sum_i^{-1}$ = its inverse matrix

m_i = mean vector

After implementation of the algorithm on the NOAA AVHRR images we obtained the classification for all pixels. Similarly working with IRS data covering JCF, the following eight major Land cover categories were identified:

Table 2. Distribution of land-use in JCF (2010)

Land-Use Type	Area (Sqkm)	Area (%)
Settlement	65.08	17.02
Agriculture land	130.48	34.12
Plantation	7.42	1.94
Sparse vegetation	2.94	0.77
Degraded vegetation	89.22	23.33
Barren land	45.31	11.85
Tanks/Ponds	8.79	2.30
Stream/River	13.10	3.43
Active mining area (Quarries+OB dumps)	20.03	5.24
Total Area	382.37	100.0
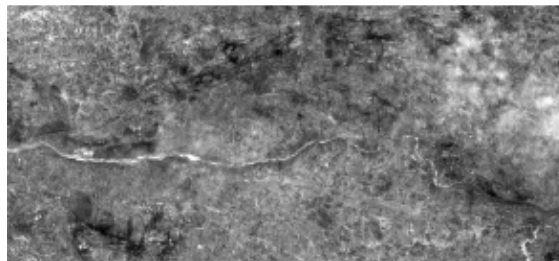
Fig.2: R1 image of JCF
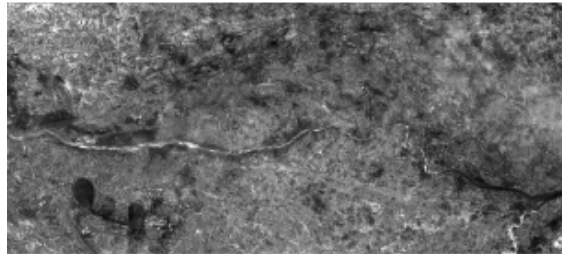
Fig.3 : R2 image of JCF
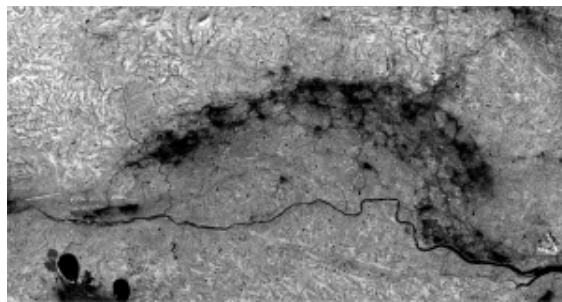
Fig.4 : R3 image of JCF
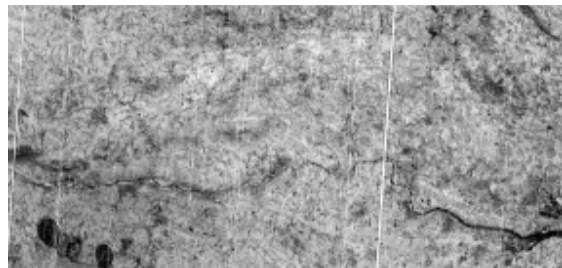
Fig.5 : NDVI image of JCF
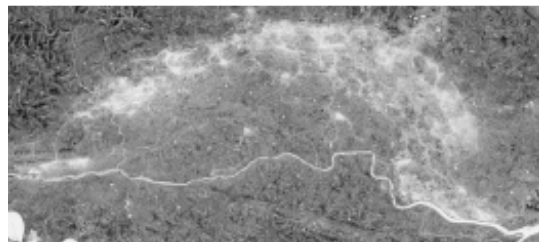
Fig.6 : MSAVI image of JCF
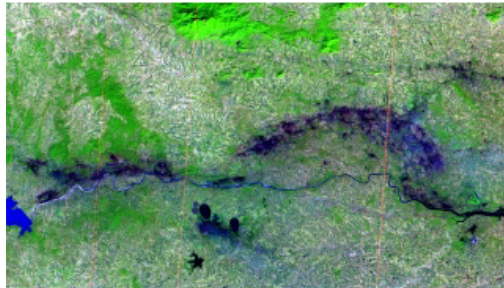
Fig.7: FCC432 image of JCF
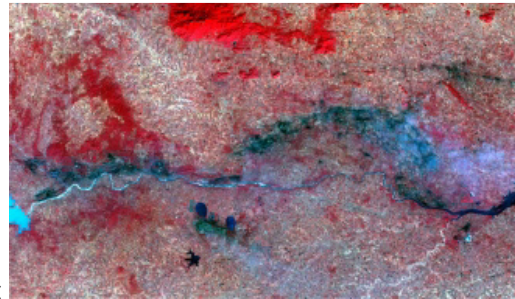
Fig.8: FCC321 image of JCF
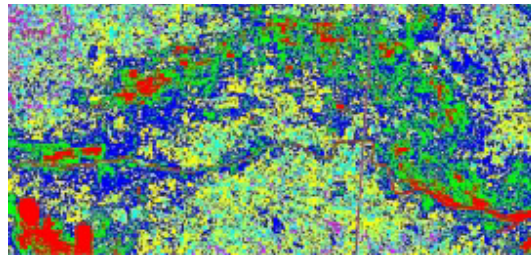
Fig. 9 : Unsupervised land cover classification of JCF
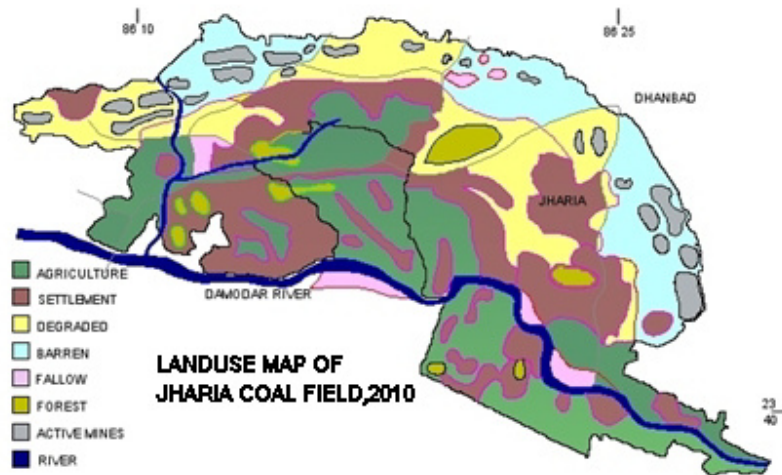
Fig.10 : Final land cover of JCF derived from maximum likelihood algorithm

Taking the area around Jharia, fluctuations in land surface temperature at day and night were analyzed for different land cover types by NOAA thermal band data and land use data. Land surface temperature at day and night was evaluated from AVHRR Band 3, 4 and 5 data (eq.1) for day and night. Land cover data was obtained from assessment of the LST and NDVI values. The following estimations were made: Areas which have low NDVI value throughout the year are built-up area; areas which have high NDVI value throughout the year are evergreen forest. The Land surface of the mining areas was observed to be higher than the other areas. The degraded vegetation has a very low temperature in night as compared to the day time temperature. Using these annual changes of NDVI values, land cover was classified.

Assessment of thermal characteristics for different land cover types was done to correlate the land covers to the thermal data. Table 1 indicates the average temperature for different land cover categories which is calculated from AVHRR band 4. In Table 4 parameters Td4 and Tn4 show the temperature at day and night derived from AVHRR band 4, and $\Delta T4$ shows the temperature difference between day and night. In Table 1 it is clearly indicated that the forest area has low temperature difference between day and night. The mine areas have distinct high temperature in day and night images.
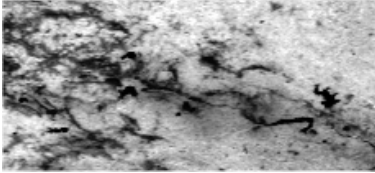
Fig.11: NOAA AVHRR image of JCF
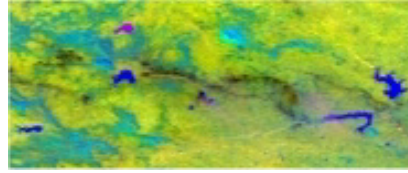
Fig.12: FCC of JCF
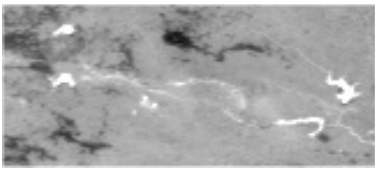

Fig.13: NDVI image of JCF
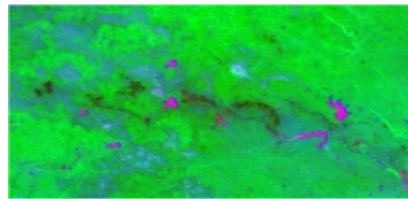
Fig.14: FCC image of JCF (to distinguish water and mines)
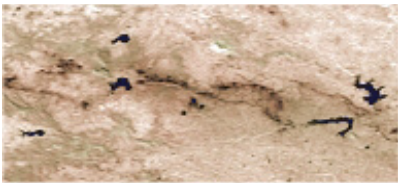
Fig.15: Enhanced image of JCF
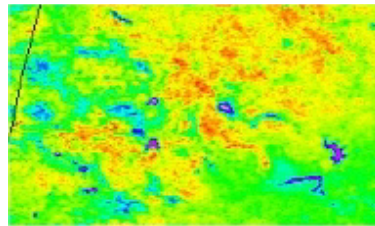
Fig.16: LST of JCF
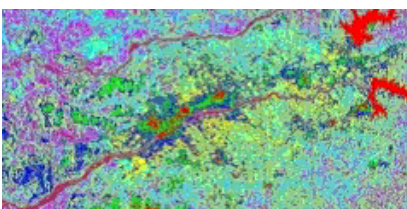
Fig.17: Land cover obtained from NOAA AVHRR

Data for the 20 images were used to train a regression model with the temperatures as parameters. The model obtained gave the following values for the temperatures for a classification accuracy of about 70.1%.

Table 3-Average of Td, Tn, ΔT of band 4 for each category

	Average		
Category	Td4 (°C)	Tn4 (°C)	ΔT4 (°C)
Settlement	24.5	19.9	5.6
Active mining area (Quarries+OB dumps)	30.1	27.8	2.3
Agriculture land	28.8	20.0	8.9
Barren	22.8	18.2	5.9
Fallow land	26.0	19.5	6.8
Water Stream/River	20.9	15.6	5.3
Forest	24.4	18.7	5.9
Degraded vegetation	27.7	19.7	8.1

The obtained land covers from both IRS and NOAA data have been compared. The NOAA AVHRR gives a performance of approximately 70.1% in the estimation of land cover when compared to the IRS LISS-III data.

Table 4 – Comparison of land cover from IRS and NOAA AVHRR

CLASS	VALUE OF COVER WITH IRS IMAGE (%)	VALUE OF COVER WITH NOAA AVHRR IMAGE (%)
Fallow land	1.2021%	0.06%
River/Water Bodies	9.9958%	9.01%
Forest	6.1924%	3.31%
Barren	13.4195%	9.87%
Settlement	20.2984%	21.64%

Agriculture	20.6755%	29.01%
Degraded	15.2927%	19.03%
Mining area/OBC	12.9237%	8.05%

6. Conclusions

Dense vegetation is abundant in the region. Areas, which can be excluded from the demarcated zone are therefore very large. Vegetation exclusion reduces the delineated zone from 3178 to 778 km2. The remaining area considered as a coal fire risk area contains only 1.48 % of the whole scene input into the knowledge based test sequence.

The average of night time temperature for most land-use categories have similar value. On the other land there is significant difference in the average of day time temperature for most land-use categories. Thus the difference of temperature between day and night is dominated by the day time temperature. One distinct pattern observed is that while the average of day time temperature for Forest is low, that for Crop land is significantly higher. It demonstrates that conversion of land from forest to grassland and agriculture effects in the increase in the day time temperature. Overall, the results of the study are quite positive. The dataset produced for this project has several deficiencies mostly dealing with issues of resolution. Increased frequency in temporal resolution offers the most promise for improving agricultural studies. An increase in spectral resolution: hyper-spectral sensors, or the addition of thermal IR data, will also improve future agricultural land-use mapping projects. Fine spectral detail will allow analysts to detect subtle differences between and within various crop types, making it feasible to conduct large-scale studies of crop varieties.

References

1. Becker F. and Li Z.L., (1990). Towards a local split window method over land surfaces, *International Journal of Remote Sensing*, **11**, 360-393.

2. Dingle Robertson, L., & King, D. J. (2011). Comparison of pixel- and object-based classification in land cover change mapping. International Journal of Remote Sensing, 32(6), 1505–1529.

3. Gislason, P. O., Benediktsson, J. A., & Sveinsson, J. R. (2006). Random Forests for land cover classification. Pattern Recognition Letters, 27(4), 294–300.

4. Henderson-Sellers, A., and Pitman, A. J., 1992, Land-surface schemes for future climate models: specification, aggregation and heterogeneity. *Journal of Geophysical Research*, **97,** 2678 - 2696.

5. Huang, C., Davis, L. S., & Townshend, J. R. G. (2002). An assessment of support vector machines for land cover classification. International Journal of Remote Sensing, 23(4), 725–749.

6. Lambin, E. F., and Ehrlich, D., 1995, Combining vegetation indices and surface temperature for land-cover mapping at broad spatial scales. *International Journal of Remote Sensing*, **16,** 573 - 579.

7. Lambin, E. F., and Ehrlich, D., 1996, The surface temperature-vegetation index space for land cover and land-cover change analysis. *International Journal of Remote Sensing*, **17,** 463 - 487.

8. Lambin, E. F., and Strahler, A. H., 1994, Indicators of land-cover change for change-vector analysis in multi-temporal space at coarse spatial scales. *International Journal of Remote Sensing*, **15,** 2099 - 2119.

9. Loveland, T. R., Merchant, J. W., Ohlen, D. O., and Brown, J., 1991, Development of a land-cover database for the conterminous U.S. *Photogrammetric Engineering and Remote Sensing*, **57,** 1453- 1463.

10. Nelson, R., and Holben, B., 1986, Identifying deforestation in Brazil using multi-resolution satellite data. *International Journal of Remote Sensing*, **7,** 429 - 448.

11. Pal, M. (2005). Random forest classifier for remote sensing classification. International Journal of Remote Sensing, 26(1), 217.

12. Sobrino, J. A., Li, Z.-L., Stoll, M. P., and Becker, F., 1994, Improvement in the Split-Window Technique for Land Surface Temperature Determination. *IEEE Transactions on Geoscience and Remote Sensing*, **32,** 243 -253.

13. Sobrino, J. A., Li, Z.-L., Stoll,M. P., and Becker, F., 1996,Multi-channel and multi-angle algorithms for estimating sea and land surface temperature with ATSR data. *International Journal of Remote Sensing*, **17,** 2089 - 2114.

14. Sobrino, J. A., Raissouni, N., and Lobo, A., 1997 a, Monitoring the Iberian Peninsula land cover using NOAA AVHRR data. In *Physical Measurements and Signatures in Remote Sensing*, edited by Gearard Guyot and Thierry Phulpin (Rotterdam: Balkema), ISBN 90 5410 919 X, pp. 787- 794.

15. Townshend, J. R., Justice, C. O., and Kalb, V., 1987, Characterization and classification of South American land cover types using satellite data. *International Journal of Remote Sensing*, **8,** 1189 -1207.

16. Tucker, C. J., Dregne, H. E., and Newcomb, W. W., 1991, Expansion and contraction of the Sahara desert from 1980 to 1990. *Science*, **253,** 299 -301.